Investigation of a silicon-based one-dimensional phononic crystal plate via the super-cell plane wave expansion method*

Zhu Xue-Feng(祝雪丰)[a], Liu Sheng-Chun(刘盛春)[b], Xu Tao(徐 涛)[a], Wang Tie-Hai(王铁海)[a], and Cheng Jian-Chun(程建春)[a]†

[a] *Key Laboratory of Modern Acoustics, MOE, and Institute of Acoustics, Nanjing University, Nanjing* 210093, *China*
[b] *Institute of Fibre Optics, Heilongjiang University, Harbin* 150080, *China*

(Received 15 June 2009; revised manuscript received 15 August 2009)

The super-cell plane wave expansion method is employed to calculate band structures for the design of a silicon-based one-dimensional phononic crystal plate with large absolute forbidden bands. In this method, a low impedance medium is introduced to replace the free stress boundary, which largely reduces the computational complexity. The dependence of band gaps on structural parameters is investigated in detail. To prove the validity of the super-cell plane wave expansion, the transmitted power spectra of the Lamb wave are calculated by using a finite element method. With the detailed computation, the band-gap of a one-dimensional plate can be designed as required with appropriate structural parameters, which provides a guide to the fabrication of a Lamb wave phononic crystal.

Keywords: Lamb wave, phononic crystal, super-cell plane wave expansion, band structures

PACC: 4320, 4335, 4390, 6290

1. Introduction

Recently, artificial materials with absolute elastic forbidden bands have aroused more and more interest in the physical, chemical and biological domains.[1−3] Of these, composite materials made of a periodic array of inclusions embedded in a silicon matrix are of unique importance for the potential combination with fully-developed semiconductor fabrication technology. The perfect blockade to elastic waves of certain frequencies promises applications in acoustic filters and high efficient acoustic couplers and waveguides, which can be further used to build novel acoustic wave circuits in the future. Currently, the band-gaps of silicon based one-dimensional (1D) and two-dimensional (2D) Lamb wave phononic crystals have been studied widely both in theory and in experiment. Chen *et al.*[4] demonstrated the existence of stopbands for lower-order Lamb waves in a silicon-based 1D composite thin plate with no substrate. Gao *et al.*[5,6] studied in detail the effect of substrate as well as the quasiperiodic system in a silicon based 1D phononic crystal layer. Vasseur *et al.*[7] published a detailed report of completed forbidden bands and waveguiding in 2D silicon-based phononic crystal plates. Mohammadi *et al.*[8,9] used experimental evidence to prove the existence of large high frequency complete phononic band gaps in silicon-based 2D plates and then further to fabricate high-Q micromechanical resonators by using a 2D phononic crystal plate.

The band-gap structures of Lamb waves are quite different from those of bulk waves (BW) and surface acoustic waves (SAW) in consideration of the upper and nether free boundary conditions. From the computational point of view, it is much more complicated and requires a large amount of time and computer resources when the traditional plane wave expansion (PWE) method as well as the virtual plane wave expansion (V-PWE) method is used. In the present paper, we employ a conversional three-dimensional (3D) plane wave expansion method,[7,10] which is also referred to as the super-cell plane wave expansion method (super-cell PWE), to study the Lamb wave propagation in a 1D phononic crystal plate with/without uniform substrate. This method converts a 1D periodic system into an imaginary 2D periodic system by stacking the plates and low impedance

*Project supported by the National Natural Science Foundation of China (Grant Nos. 10874086 and 10834009) and the National Basic Research Program of China (Grant No. 2010CB327803).
†Corresponding author. E-mail: jccheng@nju.edu.cn
© 2010 Chinese Physical Society and IOP Publishing Ltd

medium (LIM) alternately, which bypasses the upper and the nether free boundary conditions in a skilful manner and largely reduces the computational complexity. The validity of super-cell PWE is then tested via a finite element method (FEM) by comparing the transmitted power spectra (TPS) of the Lamb wave with the calculated band structure. With the super-cell PWE method, we study in detail the relationship between band gap and structural parameters such as filling factor, lattice constant to layer thickness ratio as well as the substrate thickness. Numerical study shows that the band-gap of the plate can be large enough with using appropriate structural parameters, which can be used as a reference in the fabrication of a silicon-based 1D phononic crystal plate.

2. Formulations

As shown in Fig. 1, we establish a 3D model in Cartesian coordinates to calculate the elastic band structures of 1D phononic crystal plates, where A is the inclusion gold, which can be easily processed in traditional microelectronic device fabrication, B the matrix silicon, C the LIM layer, and D the substrate. The material constants of crystalline gold used in the super-cell PWE calculations are $\rho = 19200$ kg/m^3, $C_{11} = 192.5 \times 10^9$ N/m^2, $C_{12} = 163 \times 10^9$ N/m^2, and $C_{44} = 42.4 \times 10^9$ N/m^2,[11] and those of anisotropic matrix silicon are $\rho = 2331$ kg/m^3, $C_{11} = 165.78 \times 10^9$ N/m^2, $C_{12} = 63.94 \times 10^9$ N/m^2, and $C_{44} = 79.62 \times 10^9$ N/m^2. The material constants used in the FEM calculations are $E_{\rm A} = 7.95 \times 10^{10}$ N/m^2, $G_{\rm A} = 2.78 \times 10^{10}$ N/m^2, $\sigma_{\rm A} = 0.42$ (Poisson's ratio) for gold and $E_{\rm B} = 1.30 \times 10^{11}$ N/m^2, $G_{\rm B} = 0.79466 \times 10^{11}$ N/m^2, $\sigma_{\rm B} = 0.2783$ (Poisson's ratio) for anisotropic (100) silicon.[12]

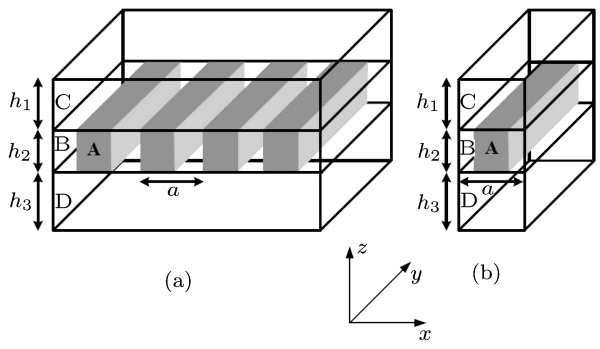


Fig. 1. (a) 1D Lamb wave phononic crystal sandwiched between two layers of homogeneous materials, and (b) 3D super-cell used in the computation.

The LIM is an imaginary material with a relatively low elastic modulus that approximately meets the requirements for a free boundary condition and an extremely low mass density, which leads the sound speed in the LIM to be much larger than that in usual solid material. In this paper, the LIM is assumed to be an isotropic material with $C_{11} = 2 \times 10^6$ N/m^2, $C_{44} = 1 \times 10^6$ N/m^2, $C_{12} = 0$ N/m^2 and $\rho = 1 \times 10^{-4}$ kg/m^3. The choice of such unphysical high sound speeds for the LIM is in good agreement with the numerical condition derived by Tanaka *et al.*[13] With these values, both good numerical convergence and computing accuracy can be achieved. The thickness of the plate, h, is assumed to be 2 mm and $h = h_2 + h_3$ where $h_3 = 0$ mm for the case without substrate. The thickness of the LIM layer, h_1, is assumed to be $5h_2$ to reduce unexpected wave coupling between two nearest-neighbour phononic layers in the z direction.[10] In the absence of body force and strain in the y direction, the SH mode wave in the 1D plate can be decoupled. Regardless of the wave propagating in the y direction, the elastic wave equations of the phononic crystal are given by

$$\rho(\boldsymbol{r})\ddot{u}_p = \partial_q[C_{pqmn}(\boldsymbol{r})\partial_n u_m] \quad (p = 1, 2, 3), \tag{1}$$

where $\boldsymbol{r} = (x, z)$. This equation can be solved by a standard Fourier expansion to $\rho(\boldsymbol{r})$, $C_{pqmn}(\boldsymbol{r})$ and $u(\boldsymbol{r}, t)$ are both position-dependent values. For convenience, let $\alpha = (\rho, C_{pqmn})$ and then we can obtain the following equations:

$$\alpha(\boldsymbol{r}) = \sum_{G_x}\sum_{G_z} \alpha_{\boldsymbol{G}} \exp[\mathrm{i}(G_x x + G_z z)], \tag{2}$$

$$u(\boldsymbol{r}, t) = \sum_{G_x}\sum_{G_z} u_{\boldsymbol{G}} \exp[\mathrm{i}(G_x x + G_z z)]\mathrm{e}^{\mathrm{i}(\boldsymbol{k}\cdot\boldsymbol{r} - \omega t)}, \tag{3}$$

where $\boldsymbol{k} = (k_x, k_z)$ is the Bloch wave vector and the 2D reciprocal-lattice vector $\boldsymbol{G} = (G_x, G_z)$. Substituting Eqs. (2) and (3) into wave equation (1), we can obtain

$$\omega^2 \begin{pmatrix} \rho_{\boldsymbol{G}-\boldsymbol{G}'} & & \\ & \rho_{\boldsymbol{G}-\boldsymbol{G}'} & \\ & & \rho_{\boldsymbol{G}-\boldsymbol{G}'} \end{pmatrix} u_{\boldsymbol{G}'} = \begin{pmatrix} M^{11}_{\boldsymbol{G},\boldsymbol{G}'} & M^{12}_{\boldsymbol{G},\boldsymbol{G}'} & M^{13}_{\boldsymbol{G},\boldsymbol{G}'} \\ M^{21}_{\boldsymbol{G},\boldsymbol{G}'} & M^{22}_{\boldsymbol{G},\boldsymbol{G}'} & M^{23}_{\boldsymbol{G},\boldsymbol{G}'} \\ M^{31}_{\boldsymbol{G},\boldsymbol{G}'} & M^{32}_{\boldsymbol{G},\boldsymbol{G}'} & M^{33}_{\boldsymbol{G},\boldsymbol{G}'} \end{pmatrix} u_{\boldsymbol{G}'}. \tag{4}$$

The explicit expressions of the matrix elements $M^{lm}_{\mathbf{G},\boldsymbol{G}'}$, $(l = m = 1, 2, 3)$ are listed in Appendix A. As shown in Eq. (4), the characteristic frequency ω is exactly the squared generalized eigenvalue of the

density matrix and elastic constant matrix. The coefficients $C^{pq}_{\boldsymbol{G}-\boldsymbol{G}'}$ and $\rho_{\boldsymbol{G}-\boldsymbol{G}'}$ are related through the following equation:

$$\alpha_{\boldsymbol{G}-\boldsymbol{G}'} = \frac{1}{V_c}\iiint_{(\text{super}-\text{cell})} \alpha(\boldsymbol{r}) \times \exp[-\mathrm{i}(\boldsymbol{G}-\boldsymbol{G}')\cdot\boldsymbol{r}]\mathrm{d}^3\boldsymbol{r}, \quad (5)$$

where V_c is the volume of the super-cell. With the above-mentioned equations, we can easily obtain the band structure of the 1D phononic crystal plate.

3. Numerical simulations by the super-cell PWE method

To guarantee convergence and accuracy of the summation in Eqs. (2) and (3), the x-component and the z-component of the reciprocal-lattice vector, i.e. $G_x = (\pm6, \pm5, \pm4, \pm3, \pm2, \pm1, 0)2\pi/a$ and $G_z = (\pm6, \pm5, \pm4, \pm3, \pm2, \pm1, 0)2\pi/h_w$, are chosen in this paper, where $h_w = h_1 + h_2 + h_3$. Previous studies[14] have shown that the main band gap width (B) of a Lamb wave phononic crystal is related to the filling factor of inclusion (f), the ratio of lattice constant to layer thickness (a/h_2) and the substrate thickness (h_3), separately. We can then simply express the main band gap width as a function, that is, $B = F(f, a/h_2, h_3)$. For $h_2 + h_3 = 2$ mm, we can further take the form, that is, $B = F(f, a/h_2, 2-h_2)$. In this paper, we promote a searching procedure to find out the relatively large value of B by tuning the three parameters $(f, a/h_2, h_3)$ in order. Firstly, we set $a/h_2 = 1$, $h_3 = 0$ and then by tuning f from 0 to 1, the main band gap widths are obtained as shown in Fig. 2(a), including two parts: part 1 and part 2.

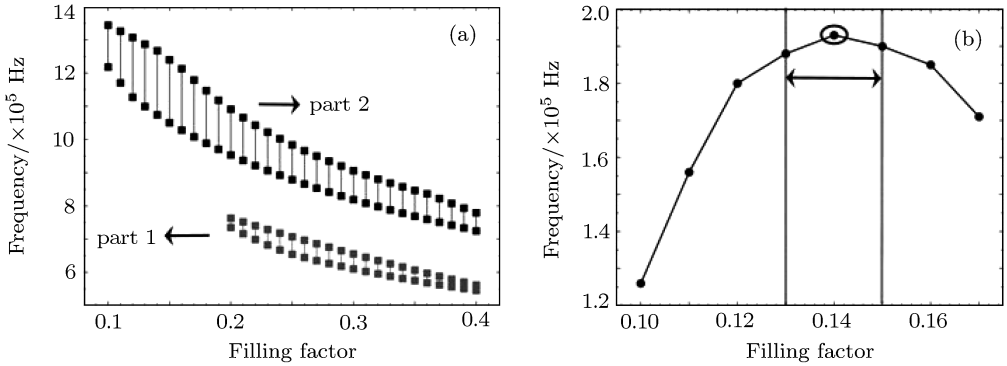


Fig. 2. (a) Relationship between band gap and filling factor, (b) band gap widths in part 2 with different filling factors ranging from 0.1 to 0.17.

In part 1 ($f = 0.2$–0.4), a small band gap is opened in the low frequency zone whereas its width is narrower than that of the band gap in part 2. The band gap width in part 2 ($f = 0.1$–0.4) locates in the high frequency zone with a larger band gap width. On the whole, we can see that as the filling factor becomes smaller the location of the band gap moves towards the high frequency zone, which accords with the previous results very well.[15] The band gap widths with different filling factors are then plotted in Fig. 2(b), in which the appropriate filling factor should be in a range from 0.13 to 0.15 and we choose $f = 0.14$ as our selected parameter (marked with the elliptic frame). Figure 3(a) shows the relationship between the ratio of lattice constant to layer thickness, (a/h_2), and acoustic band gap when $f = 0.14$ and $h_3 = 0$. Figure 3(b) shows the band gap widths with different values of a/h_2. As shown in Fig. 3, the acoustic band gap shifts towards the high frequency zone as the a/h_2 becomes smaller and the appropriate a/h_2 value should be in the region from 0.7 to 0.8 when $f = 0.14$ and $h_3 = 0$. Hereon we choose $a/h_2 = 0.7$ as the selected value (marked with rectangular frame) both for the largest one plotted and for the convenience of FEM simulation by noting that $f = 0.14 \approx 1/7$.

As seen in Fig. 4(b), the band gap width remains stable as the substrate thickness changes from 0 to 0.25 mm and then decreases rapidly with the band gap shifting towards the high frequency zone. The turning point 0.25 mm is marked with a triangular frame. It is easily understood that as the thickness of the phononic crystal layer (h_2) decreases, the band gap shifts towards the high frequency zone with its band gap width increasing proportionally. However, the increase of substrate thickness (h_3) allows more modes to pass (especially high

frequency modes) as seen in Fig. 4(a), which acts much like a wave-leaking channel. In conclusion, these two competitive factors will lead the band gap width to be stable and then fall off steeply, and the turning point is a key factor for the fabrication process.

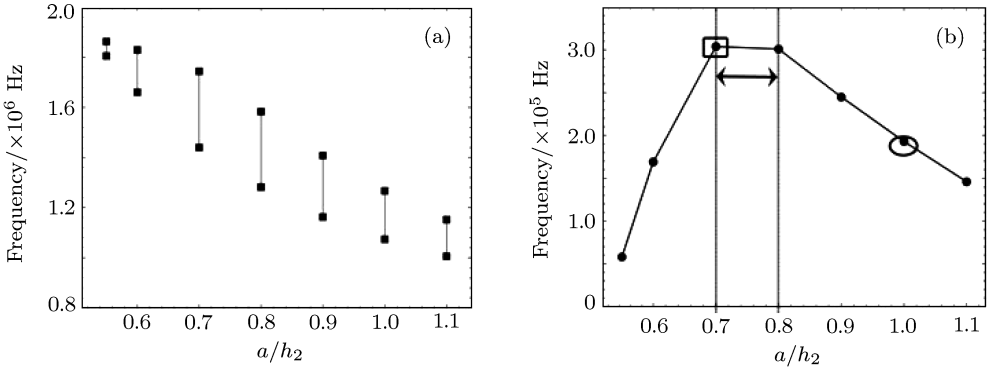


Fig. 3. (a) Relationship between acoustic band gap and a/h_2 ratio, and (b) band gap widths with different values of a/h_2 ratio ranging from 0.55 to 1.1.

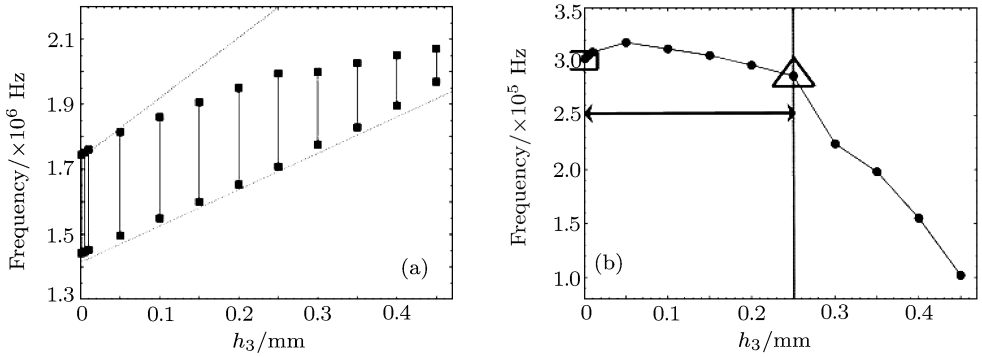


Fig. 4. (a) Relationship between acoustic band gap and substrate thickness (h_3), and (b) band gap widths with different values of substrate thickness (h_3) ranging from 0 to 0.45 mm.

4. Numerical simulation by the finite element method

We use FEM to test the validity of this super-cell PWE method. For good computational reliability, we use ANSYS 11.0 to build up the model, in which the thickness of the plate is set to be 2 mm (no substrate: $h_2 = 2$ mm, $h_3 = 0$ mm) and 2.2 mm (with substrate: $h_2 = 2$ mm, $h_3 = 0.2$ mm). The lattice constant a is determined to be 1.4 mm by noting that $a/h_2 = 0.7$ and filling factor $f = 1/7$. In the model, the length of the plate is set to be 600 mm, with the number of inclusions being 43. All the inclusions are embedded periodically in the middle of the plate. The exciting source is set to be 5 mm from the left edge in distance. A 2D viscous-spring artificial boundary is used to reduce the reflected wave from the two edges in maximum and element size is assumed to be 1/10000 m. The source force is discretized both in space (Guassian distribution) and in time (triangle distribution). After collecting the time-varying horizontal displacement of a node selected near the super-lattice structure, we let it be Fourier transformed to obtain the TPS map.

Figure 5 shows the dispersion curve and TPS for the 1D composite structure plate both with and without substrates. For the case without substrate, we can see that the band gap with designated parameters locates between 1.431 MHz and 1.737 MHz from the band structure map. The calculated TPS map shows that an obvious gap exists between 1.432 MHz and 1.638 MHz for the Lamb wave modes, which is agreeable but somewhat narrower. This may be due to the finite periods ($N = 43$). The finite periods cannot block all the modes between 1.431 MHz and 1.737 MHz completely (especially high frequency modes) but only reduce the mode intensity between 1.432 MHz and 1.638 MHz a great deal. For the case with substrate, the band gap with appointed parameters locates between 1.479 MHz and 1.751 MHz from the band structure map. The

calculated TPS map shows an obvious gap between 1.480 MHz and 1.604 MHz, which also matches well. We also find out that the band gap width in Fig. 5(c) or Fig. 5(d) is narrower than that in Fig. 5(a) or Fig. 5(b) correspondingly, which can be explained by the fact that the existing substrate is acting as a wave-leaking channel and consequently can make the band gap width decrease rapidly.

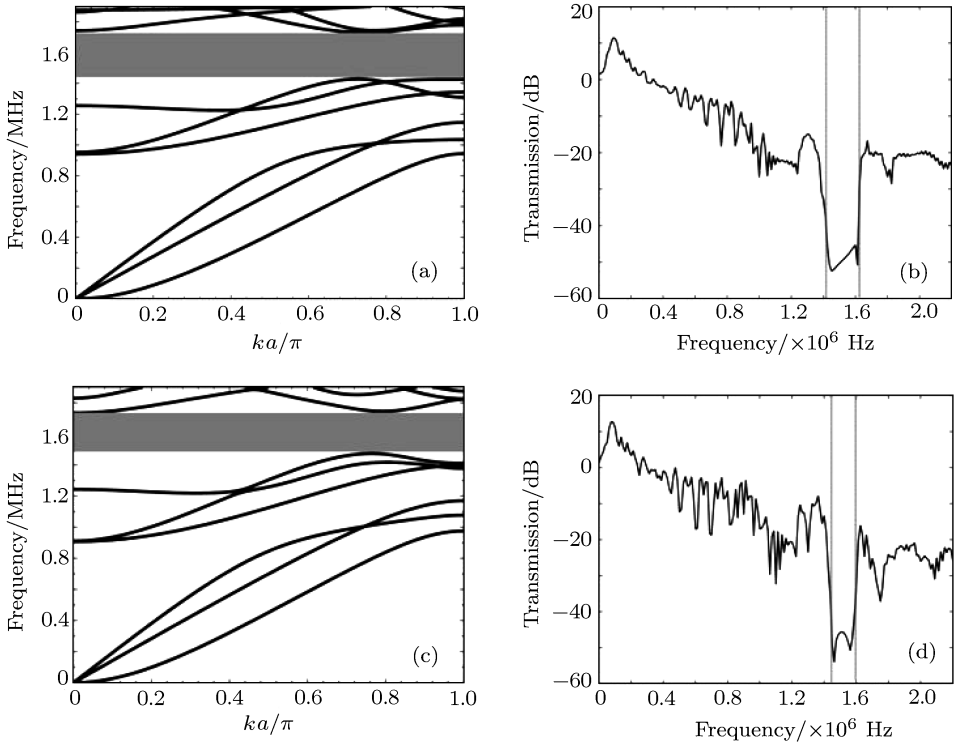


Fig. 5. (a) Dispersion curves of Lamb wave modes for the 1D plate without substrate, (b) TPS computed by the FEM ($f = 1/7$, $a/h_2 = 0.7$, $h_2 = 2$ mm, $h_3 = 0$ mm), (c) dispersion curves of Lamb wave modes for the 1D plate with substrate, and (d) TPS computed by the FEM ($f = 1/7$, $a/h_2 = 0.7$, $h_2 = 2$ mm, $h_3 = 0.2$ mm).

5. Conclusions

In conclusion, we employ the super-cell PWE method to study the band structures of lower-order Lamb wave modes propagating in a silicon-based 1D periodic composite plate with and without substrates, and then use the FEM to prove its validity. By tuning the structural parameters in the promoted searching procedure, we obtain their relationships with band gap widths. We can design the band-gap width of the 1D Lamb wave phononic crystal plate as required with appropriate structural parameters (f, a/h_2, h_3), and our work provides theoretical guidance for the experimental fabrication in the future.

Appendix A

The expressions of elements of the matrix $M^{lm}_{\boldsymbol{G},\boldsymbol{G}'}$, $(l = m = 1, 2, 3)$ are expressed as

$$
\begin{aligned}
&M^{11}_{\boldsymbol{G},\boldsymbol{G}'} = C^{11}_{\boldsymbol{G}-\boldsymbol{G}'}(k_x + G'_x)(k_x + G_x) + C^{44}_{\boldsymbol{G}-\boldsymbol{G}'}\, G'_z G_z, \quad M^{12}_{\boldsymbol{G},\boldsymbol{G}'} = 0,\\
&M^{13}_{\boldsymbol{G},\boldsymbol{G}'} = C^{12}_{\boldsymbol{G}-\boldsymbol{G}'}\, G'_z(k_x + G_x) + C^{44}_{\boldsymbol{G}-\boldsymbol{G}'}(k_x + G'_x)G_z, \quad M^{21}_{\boldsymbol{G},\boldsymbol{G}'} = 0,\\
&M^{22}_{\boldsymbol{G},\boldsymbol{G}'} = C^{44}_{\boldsymbol{G}-\boldsymbol{G}'}(k_x + G'_x)(k_x + G_x) + C^{44}_{\boldsymbol{G}-\boldsymbol{G}'}\, G'_z G_z, \quad M^{23}_{\boldsymbol{G},\boldsymbol{G}'} = 0,\\
&M^{31}_{\boldsymbol{G},\boldsymbol{G}'} = C^{44}_{\boldsymbol{G}-\boldsymbol{G}'}\, G'_z(k_x + G_x) + C^{12}_{\boldsymbol{G}-\boldsymbol{G}'}(k_x + G'_x)G_z, \quad M^{32}_{\boldsymbol{G},\boldsymbol{G}'} = 0,\\
&M^{33}_{\boldsymbol{G},\boldsymbol{G}'} = C^{44}_{\boldsymbol{G}-\boldsymbol{G}'}(k_x + G'_x)(k_x + G_x) + C^{11}_{\boldsymbol{G}-\boldsymbol{G}'}\, G'_z G_z,
\end{aligned}
$$

where the Fourier coefficients $C^{pq}_{\boldsymbol{G}-\boldsymbol{G}'}$ are related to $C_{pqmn}(\boldsymbol{r})$ in a conventional manner.

References

[1] Wang G, Shao L H, Liu Y Z and Wen J H 2006 *Chin. Phys.* **15** 1843

[2] Yu D L, Wang G, Liu Y Z, Wen J H and Qiu J 2006 *Chin. Phys.* **15** 266

[3] Zhao H G, Wen J H, Liu Y Z, Yu D L, Wang G and Wen X S 2008 *Chin. Phys.* B **17** 1305

[4] Chen J J, Zhang K W, Gao J and Cheng J C 2006 *Phys. Rev.* B **73** 094307

[5] Gao J, Cheng J C and Li B W 2007 *Appl. Phys. Lett.* **90** 111908

[6] Gao J, Zou X Y, Cheng J C and Li B W 2008 *Appl. Phys. Lett.* **92** 023510

[7] Vasseur J O, Deymier P A, Djafari-Rouhani B, Pennec Y and Hladky-Hennion A C 2008 *Phys. Rev.* B **77** 085415

[8] Mohammadi S, Eftekhar A A, Khelif A, Hunt W D and Adibi A 2008 *Appl. Phys. Lett.* **92** 221905

[9] Mohammadi S, Eftekhar A A, Hunt W D and Adibi A 2009 *Appl. Phys. Lett.* **94** 051906

[10] Hou Z L and Assouar B M 2008 *Phys. Lett.* A **372** 2091

[11] Hsu J C and Wu T T 2006 *Phys. Rev.* B **74** 144303

[12] Lackner T 1989 *J. Electron. Mater.* **18** 1

[13] Tanaka Y, Tomoyasu Y and Tamura S I 2000 *Phys. Rev.* B **62** 7387

[14] Chen J J, Qin B and Cheng J C 2005 *Chin. Phys. Lett.* **22** 1706

[15] Maldovan M and Thomas E L 2006 *Appl. Phys.* B **83** 595